phys. stat. sol. (a) **205**, No. 12, 2822–2830 (2008) / **DOI** 10.1002/pssa.200880452

physica status solidi a
www.pss-a.com
applications and materials science

Neodymium-doped fluorochlorozirconate glasses as an upconversion model system for high efficiency solar cells

Bernd Ahrens[1], Philipp Löper[2], Jan Christoph Goldschmidt[2], Stefan Glunz[2], Bastian Henke[3], Paul-Tiberiu Miclea[3,4], and Stefan Schweizer[*,3,4]

[1] Department of Physics, Faculty of Science, University of Paderborn, Warburger Str. 100, 33098 Paderborn, Germany
[2] Fraunhofer Institute for Solar Energy Systems, Heidenhofstr. 2, 79110 Freiburg, Germany
[3] Fraunhofer Center for Silicon Photovoltaics, Walter-Hülse-Str. 1, 06120 Halle, Germany
[4] Institute of Physics, Martin-Luther-University of Halle-Wittenberg, Heinrich-Damerow-Str. 4, 06120 Halle, Germany

Received 1 July 2008, revised 8 October 2008, accepted 8 October 2008
Published online 18 November 2008

PACS 61.05.Cp, 61.46.Hk, 78.55.Qr, 81.40.Tv, 84.60.Jt

[*] Corresponding author: e-mail stefan.schweizer@csp.fraunhofer.de, Phone: +49 345 5589128, Fax: +49 345 5589101

Thermal processing of as-made fluorozirconate glasses which were additionally doped with neodymium and chlorine ions leads to enhanced upconversion fluorescence intensities. The samples were annealed between 240 °C and 290 °C and the optimum value of upconversion intensity was found for the 270 °C sample. The development of glasses doped with Er, whose luminescence characteristics make it a better choice for application as an upconversion layer on silicon solar cells, is in progress. In addition, we present external quantum efficiency measurements of a silicon solar cell with a $NaYF_4:Er^{3+}$ upconverter. We also show a theoretical analysis where erbium transitions can be enhanced selectively to increase upconversion efficiency.

1 Introduction Low-phonon energy glasses are desirable hosts for rare-earth (RE) ions such as Er, Ho, Nd, Pr, and Tm because they enable emission from energy levels that would be quenched in high-phonon energy glasses.

Upconversion occurs when the active RE ion is optically excited to emit visible light by the sequential absorption of two low-energy infrared photons. Of particular importance to the upconversion efficiency is the intermediate energy level lifetime of the RE ion, which depends on the phonon frequency of the host material.

Fluorozirconate (FZ) glasses have low-phonon energies ($<580\ cm^{-1}$) [1] leading to reduced non-radiative losses and increased upconversion efficiencies. However, the phonon frequency is not only dependent on the composition of the matrix the RE ion is incorporated into but also on the size of the matrix; in nanocrystals only low-phonon frequencies are found [2].

Upconversion emissions are of particular interest for upconversion lasers, and also for photovoltaic applications where the efficiency of bifacial solar cells could be vastly improved by an upconverting back layer [3].

Figure 1 shows the possible design of a system with a solar cell and an upconverter on its rear side. The big advantage of upconversion is that it addresses the bottleneck of the low absorption of long wavelength light in silicon solar cells, while keeping the already highly developed solar cell itself almost unchanged. The theoretical limit for a solar cell with an upconverter illuminated by non-concentrated light is increased from close to 30% to 47.6% [3].

The first upconversion solar cell system was realised in 1996 by Gibart et al. [4] with an Yb^{3+} and Pr^{3+} doped vitroceramic and a GaAs solar cell. The authors report an efficiency of 2.5%. In Gibart's work, the upconversion is sensitized by the $^2F_{7/2} \rightarrow {}^2F_{5/2}$ transition of the Yb^{3+} ion which was pumped with 1.39 eV photons, i.e. just 30 meV below the GaAs bandgap of 1.42 eV. Shalav et al. [5], however, built the first upconversion system based on silicon solar

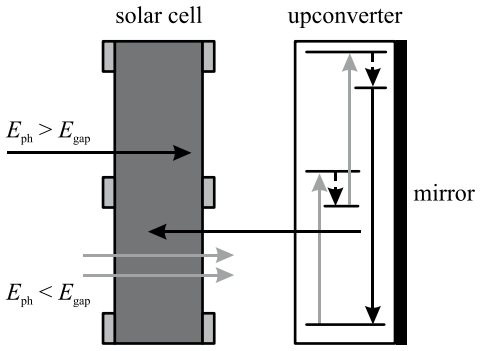

Figure 1 Bifacial solar cell with an upconverter on its rear side. Sub-bandgap photons are transmitted through the solar cell but absorbed in the upconverter which is excited successively. By recombination to the ground state, the upconverter emits a photon which can be absorbed by the solar cell.

cells and showed a response at much lower photon energies compared to Gibart's work. They report an external quantum efficiency of 3.4% at 1523 nm (0.81 eV) at an illumination intensity of 2.4 W/cm^2 for a system consisting of a bifacial silicon solar cell and a $NaYF_4:Er^{3+}$ upconverter.

In this work, we review our investigations on Nd^{3+}-doped FZ-based glasses which were additionally doped with chlorine ions. Nd^{3+} upconversion emission has to be pumped at about 800 nm (1.55 eV) and thus Nd^{3+}-based upconversion layers on the rear side of a silicon solar cell will not work since 800 nm light is absorbed by silicon itself. Nd^{3+}-doped systems, however, can serve as a model system for Er^{3+}-doped glasses or glass-ceramics. Er^{3+} exhibits energy levels that are conveniently spaced for upconversion layers for silicon solar cells.

In addition, we present our tests with a $NaYF_4:Er^{3+}$ upconverter and a bifacial silicon solar sell. Finally, we present ideas on how the upconversion efficiency can be improved by plasmon resonance.

2 Upconversion in fluorozirconate glasses and glass ceramics

In this section we describe our investigations on Nd-doped FZ glasses which were additionally doped with chlorine ions and the first results on an Er-doped FZ glass.

2.1 Samples

The Nd-doped fluorochlorozirconate (FCZ) glasses investigated are based on the well-known ZBLAN composition [6]. The nominal composition of the FCZ glasses is $(53-x)ZrF_4-10BaF_2-10BaCl_2-(20-x) \times NaCl-xKCl-3.5LaF_3-3AlF_3-0.5InF_3-xNdF_3$, where $x = 5$ (values in mole percent). The constituent chemicals were melted in a glassy carbon crucible at 745 °C in an inert atmosphere of nitrogen and then poured into a brass mold that was at a temperature of 200 °C, i.e. below the glass transition temperature of 260 °C for an FZ-based glass [6], before being slowly cooled to room temperature. The samples were subsequently brought to a temperature of 240, 250, 260, 270, 280, and 290 °C and held there for 20 minutes in an inert nitrogen atmosphere. The visible appearance of the initial FCZ glasses is transparent, but after thermal processing there is evidence of crystallization in all of the FCZ glasses, ranging from a near-transparent glass, which is light yellow in transmitted light, to one which is opaque and milky white. The samples were cut into 7 mm × 5 mm × 1 mm plates and polished.

In addition, we prepared an Er-doped FZ glass comprised of $52ZrF_4-20BaF_2-20NaF-3.5LaF_3-3AlF_3-0.5InF_3-1ErF_3$ (values in mole percent).

2.2 Setup

Fluorescence spectra were recorded using a single-beam spectrometer with a 0.55 m monochromator (Horiba Jobin Yvon iHR550). The excitation was carried out with continuous wave infrared laser diode operating at 800 nm (Nd-doped FZ glasses) or at 1540 nm (Er-doped FZ glasses); the fluorescence was detected in the visible and in the infrared spectral range with a cooled photomultiplier (Hamamatsu R943-02) and with a cooled Ge detector (Edinburgh Instruments), respectively. The spectra were not corrected for spectral sensitivity of the experimental setup.

For the time-resolved fluorescence measurements the infrared laser diode was switched on and off with a square wave signal from a generator (Rhode & Schwarz AFS); the repetition frequency was set at approximately 1 kHz. The fluorescence signal was detected with the photomultiplier and recorded with a digital oscilloscope (Tektronix TDS 1012B). For the power dependence measurements of the fluorescence and upconverted fluorescence intensities a silicon optical power meter (Thorlabs S121B) was used to measure the excitation power.

2.3 X-ray diffraction

Figure 2 shows the X-ray diffraction (XRD) data for the 5% Nd-doped FCZ glass as-made and annealed for 20 minutes at the temperatures indicated. The XRD data of the as-made sample consists of very broad peaks at about 26° and 47°, typical for glasses close to the ZBLAN formulation [8] for copper K-alpha radiation. For an annealing temperature of 240 °C (data not shown) no significant change in the XRD pattern can be observed. However, sharper peaks arise upon increasing the annealing temperature from 250 °C to 290 °C. We identify these peaks as reflections from hexagonal $BaCl_2$ (space group $P\bar{6}2m$ (189), $a = 0.8066$ nm, $c = 0.4623$ nm, bar graph (PDF #45-1313) in Fig. 2a) [9]. There is no phase transition from hexagonal to orthorhombic phase $BaCl_2$ as was found in Eu-doped FCZ glass ceramics [10, 11]. For the 290 °C annealed sample, however, there are peaks from phases which have not yet been identified; they are marked with asterisks in Fig. 2. Additional peaks from unidentified phases have also been observed in Eu-doped FCZ glass ceramics [10, 11].

The XRD peaks are wider than the instrumental resolution of 0.085°, suggesting size-broadening effects. We estimate the particle sizes by using the Scherrer formula [12].

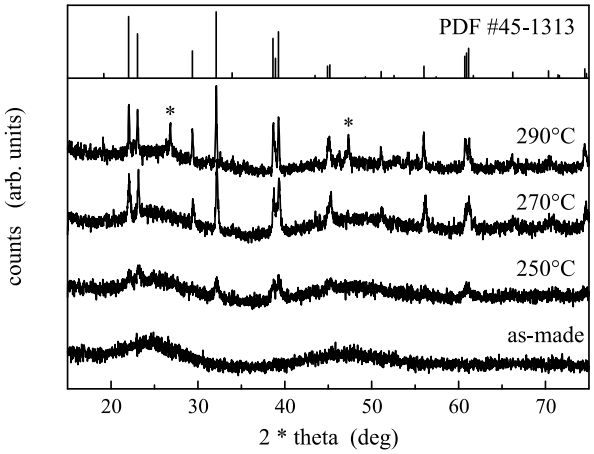

Figure 2 XRD data for the 5% Nd-doped FCZ glass ceramic, as-made and annealed, for 20 min at 250 °C, 270 °C, and 290 °C. The curves are vertically displaced for clarity; the line pattern of hexagonal phase $BaCl_2$ (PDF #45-1313) is shown for comparison. Reprinted with permission from Ref. [7]. Copyright 2008, American Institute of Physics.

We did not consider any stress or strain effects which may also lead to additional line broadening. The Scherrer formula is applied to the (201) reflection of hexagonal phase $BaCl_2$ at about 32°; the line profile is fitted by a Lorentzian. The particle diameters, after thermal processing at 250 °C, 260 °C, and 270 °C, are between 20 nm and 60 nm; for annealing temperatures at 280 °C and above the particles grow rapidly and their sizes become >100 nm (Fig. 3, open squares). The XRD linewidth of the (201) reflection for 280 °C and 290 °C annealing is too close to the instrumental resolution to allow a precise estimate of the particle size (see error bars in Fig. 3, open squares). However, the Scherrer analysis of the X-ray diffraction pattern provides a first estimate of the particle size; there is a trend to bigger particles for higher annealing temperatures. In addition, Fig. 3, full squares, shows that for annealing above 270 °C; the hexagonal phase $BaCl_2$ nano-crystals start to dissolve, i.e. the hexagonal phase $BaCl_2$ volume fraction in the glass decreases.

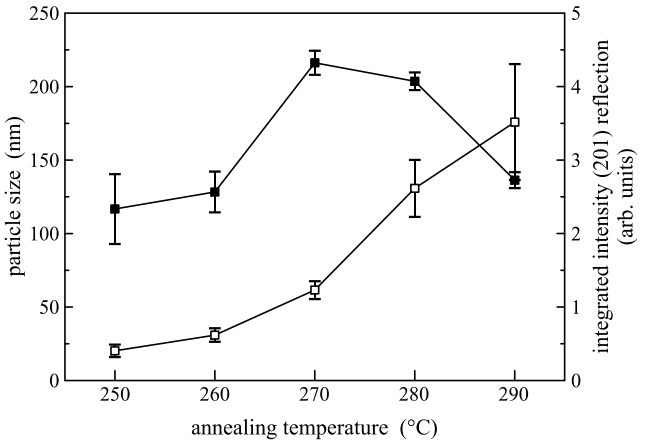

Figure 3 Particle size (open squares) and integrated intensity of the (201) reflection (full squares) vs. annealing temperature. Reprinted with permission from Ref. [7]. Copyright 2008, American Institute of Physics.

2.4 Differential scanning calorimetry The emergence of a crystalline phase in the XRD patterns after processing samples for 20 minutes at different temperatures (Fig. 2) can be correlated to the DSC data plotted in Fig. 4. The DSC data for the 1% Nd-doped FZ glass (Fig. 4a) shows a glass transition at ~262 °C in agreement with that observed in a pure FZ glass [6]. No crystallization peaks can be found upon doping the fluorozirconate glass with Nd only; however, crystallization is initiated if the glass is additionally doped with chlorine ions. Doping the FZ base glass with chlorine (Fig. 4b) shifts the glass transition temperature to ~211 °C which is significantly less than that for the FZ base glass. The exothermic peak at about 250 °C is assigned to the crystallization of hexagonal $BaCl_2$. The two peaks at ~310 °C and ~365 °C are also crystallization peaks; the latter one is also observed in pure FZ glass where the main glass crystallization starts at ~350 °C [6]. For the as-made 5% Nd-doped FCZ glass (Fig. 4c) the glass transition temperature is at ~216 °C. Interestingly, the peak for the hexagonal phase $BaCl_2$ crystallization is now at ~280 °C. The crystallization peak at 310 °C is shifted to 320 °C whereas the glass crystallization peak is now at ~335 °C.

2.5 Infrared fluorescence Figure 5 shows the infrared (IR) fluorescence spectrum of different 5% Nd-doped FCZ glass samples: as-made, annealed at 250 °C, 270 °C, and 290 °C; the spectra were recorded under continuous laser excitation at 803 nm in close resonance with the $^4I_{9/2} \rightarrow {}^4F_{5/2}$ transition of Nd^{3+} (see Fig. 6). All samples

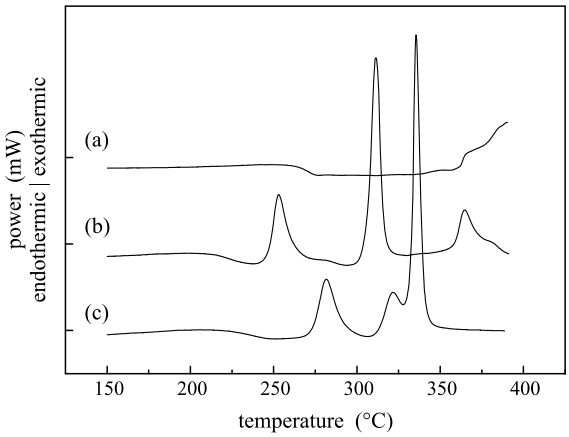

Figure 4 DSC data for (a) a 1% Nd-doped FZ glass, (b) an undoped FCZ glass ceramic, and (c) a 5% Nd-doped FCZ glass ceramic. The curves are vertically displaced for clarity. Obviously, crystallization can only be found in the chlorine co-doped samples. Reprinted with permission from Ref. [7]. Copyright 2008, American Institute of Physics.

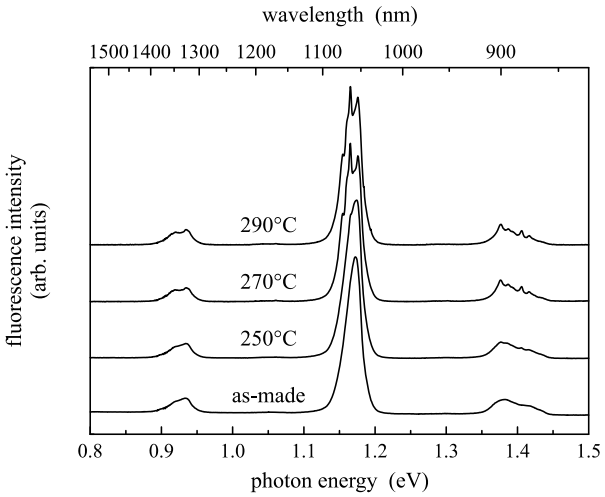

Figure 5 Fluorescence spectra for 5% Nd-doped FCZ glass ceramics: as-made, annealed at 250 °C, 270 °C, and 290 °C. The fluorescence was excited at 803 nm with a continuous wave infrared laser diode. Reprinted with permission from Ref. [7]. Copyright 2008, American Institute of Physics.

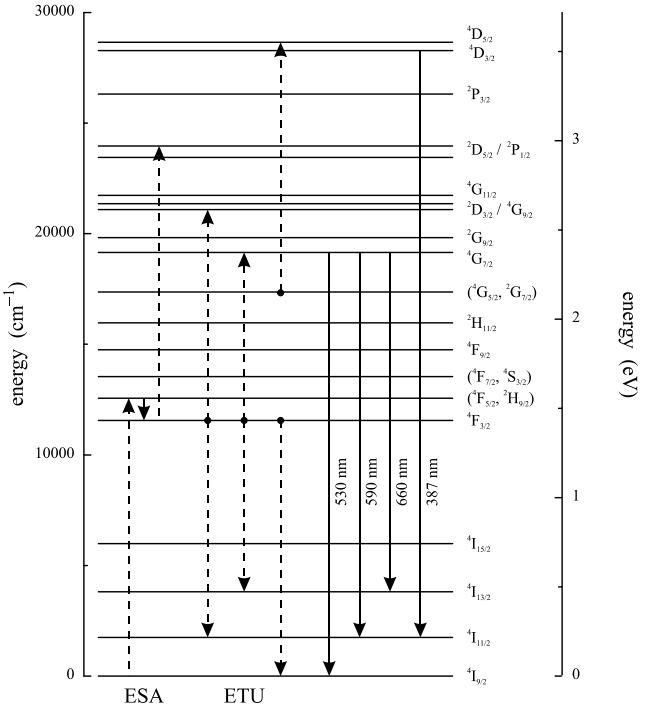

Figure 6 Energy level diagram of Nd^{3+} in FZ glasses. Possible upconversion routes (dashed arrows) and assignments of the main upconverted emission bands (solid arrows) are indicated. Reprinted with permission from Ref. [14].

show three main emission bands peaking at 885 nm, 1060 nm, and 1340 nm which can be assigned to transitions from the $^4F_{3/2}$ excited state to the $^4I_{9/2}$, $^4I_{11/2}$, and $^4I_{13/2}$ ground state of Nd^{3+}, respectively. Upon thermal processing above 250 °C all three IR emission bands start to split into several lines. The splitting results from the crystal field splitting of the $^4I_{9/2}$, $^4I_{11/2}$, and $^4I_{13/2}$ ground state [13]. The IR fluorescence intensity did not change within experimental error; the experimental resolution for the fluorescence measurements was 0.2 nm.

2.6 Upconverted fluorescence Upconversion in the visible range has been observed at room temperature under continuous wave infrared laser excitation at 803 nm. Figure 7 shows the upconverted fluorescence spectrum for the 270 °C annealed FCZ glass ceramic in the 340–750 nm spectral range. Note that at about 750 nm, scattered excitation light starts to enter the spectrum. The most intense emission bands are located in the green (530 nm), yellow (590 nm), and red (660 nm) region. They arise from the ^4G multiplets [15]. The ^4G multiplets, comprised of the $^4G_{9/2}$, $^4G_{7/2}$, and $^4G_{5/2}$ states, produce overlapping emission bands, and are therefore the strongest in the spectrum. The ^4G multiplets are energetically accessible with two 803 nm photons (Fig. 6). The weak bands in the blue spectral range originate from the $^2P_{1/2}$ excited state.

The upconverted fluorescence bands at 362 nm, 387 nm, and 418 nm are only accessible with three photons. The highest energy band at 362 nm arises from a $^4D_{3/2}$ to $^4I_{9/2}$ transition; the 387 nm emission is from the same excited state, but to the $^4I_{11/2}$ ground state (Fig. 6). The 418 nm emission can be attributed to a transition from the $^4D_{3/2}$ excited state to the $^4I_{13/2}$ ground state.

2.7 Power dependence Figure 8 shows the dependence of the emission intensity on the 803 nm excitation power for the infrared fluorescence band at 880 nm and the most intense upconverted fluorescence bands in the 270 °C annealed FCZ glass ceramic. The power dependence was measured by inserting different optical filters (e.g. neutral density filters) into the pump beam. Fluorescence spectra

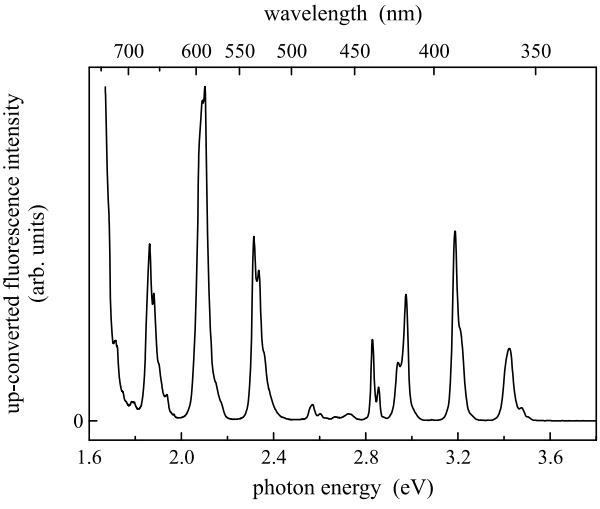

Figure 7 Upconverted fluorescence spectrum for the 270 °C sample. The upconverted fluorescence was excited at 803 nm with a continuous wave infrared laser diode. Reprinted with permission from Ref. [14].

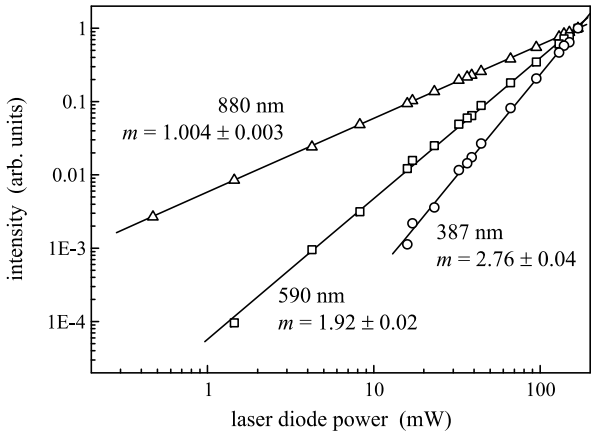

Figure 8 Normalized power dependence (in double-logarithmic scale) of the fluorescence and upconverted fluorescence intensities in the 270 °C FCZ glass ceramic sample, recorded at the wavelengths indicated under continuous wave laser diode excitation at 803 nm. Reprinted with permission from Ref. [14].

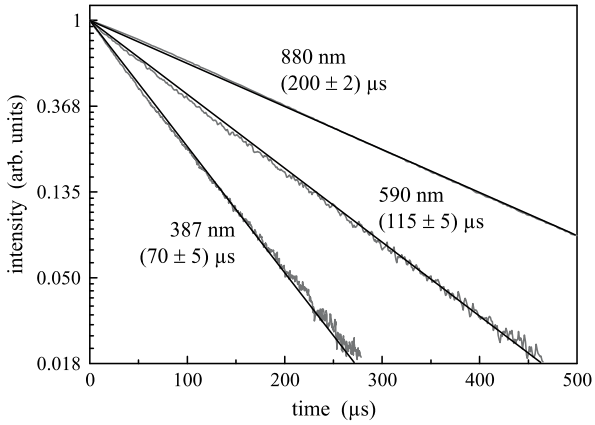

Figure 9 Normalized fluorescence decay of Nd^{3+} in the 270 °C FCZ glass ceramic. The fluorescence was detected at the wavelength indicated and excited at 803 nm with an infrared laser diode. Reprinted with permission from Ref. [14].

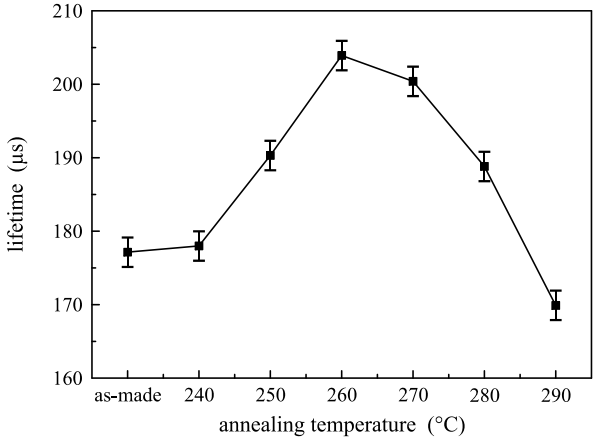

Figure 10 Decay time of the 880 nm Nd^{3+} emission in FCZ glass ceramics. The fluorescence was excited at 803 nm with an infrared laser diode. Reprinted with permission from Ref. [14].

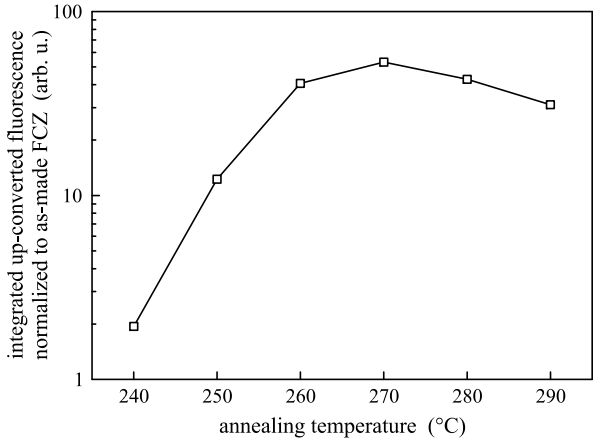

Figure 11 Upconverted fluorescence intensity vs. annealing temperature normalized to as-made FCZ. The line is a guide to the eye. Reprinted with permission from Ref. [7]. Copyright 2008, American Institute of Physics.

were recorded over several orders of magnitude of excitation power, e.g. from 170 mW (maximal LD output power) down to a few µW. For the emission at 880 nm, the slope is 1.004 ± 0.003, i.e. an almost perfect linear dependence on the excitation power without any saturation effects. Upconversion spectra were recorded for excitation powers in the range from 170 mW down to 1.5 mW. For the band at 590 nm, the slope is $m = 1.92 \pm 0.02$ which strongly suggests 2-photon upconversion processes. The bands at 530 nm and 660 nm behave similarly. The upconverted fluorescence bands of wavelengths shorter than 400 nm, i.e. in the ultraviolet spectral range, are more difficult to measure because they are smaller in intensity. However, we detected reasonable spectra for excitation powers from 170 mW down to 15 mW for the upconverted emission band at 387 nm. The slope is $m = 2.76 \pm 0.04$ and thus significantly larger than the one found for the visible upconversion bands. This indicates that we are dealing here with 3-photon upconversion processes.

2.8 Lifetime The experimental setup did not allow monitoring of the temporal development of the fluorescence and upconversion but only the delayed decay. Note, that we did not have a pulsed excitation source with a pulse width of a few nanoseconds but a laser diode which was switched on and off with a square wave signal at a repetition frequency of approximately 1 kHz; the "pulse" width was thus approximately 0.5 ms.

Figure 9 shows the normalized fluorescence decay of Nd^{3+} in the 270 °C annealed FCZ sample. The Nd^{3+} decay was recorded for the infrared fluorescence at 880 nm, the yellow, 2-photon upconverted fluorescence at 590 nm, and the ultraviolet, 3-photon upconverted fluorescence at 387 nm. The lifetime of the infrared fluorescence is (200 ± 2) µs, that of the 2-photon upconverted fluo-

rescence (115 ± 5) µs, and that of the 3-photon upconverted fluorescence (70 ± 5) µs.

As was already stated in the introduction, of particular importance to the upconversion efficiency is the intermediate energy level lifetime, specifically for the 2-photon upconversion processes the energy level lifetime of the $^4F_{3/2}$ level is important. Figure 10 shows that the lifetime of the $^4F_{3/2}$ to $^4I_{9/2}$ transition (880 nm) depends significantly on the annealing temperature: the longest lifetime was found for the 270 °C sample. This is in good agreement with the observation that the best upconversion efficiency was also found for the 270 °C FCZ sample (Fig. 11).

2.9 Erbium-doped fluorozirconate glass Fig. 12 shows the energy level diagram of Er^{3+} in FZ glasses [16, 17] along with possible upconversion routes and assignments of the main upconverted emission bands.

Upconversion in the visible range has been observed under continuous wave infrared laser excitation at 1540 nm. Figure 13 shows the upconverted fluorescence spectrum for the Er-doped FZ glass in the 400–900 nm spectral range. The most intense emission bands are located in the green (530 nm and 550 nm) and red (660 nm) region. They arise from the $^2H_{11/2}$ (530 nm), $^4S_{3/2}$ (550 nm) and $^4F_{9/2}$ (660 nm) excited states. These levels are energetically accessible with three 1540 nm photons (Fig. 12). All lines are split by about 0.03 eV which is caused by the crystal field splitting of the $^4I_{15/2}$ ground state.

The 820 nm band in the infrared spectral range arises from the $^4I_{9/2}$ state; this level is accessible with two 1540 nm photons (Fig. 12) and is also split by 0.03 eV.

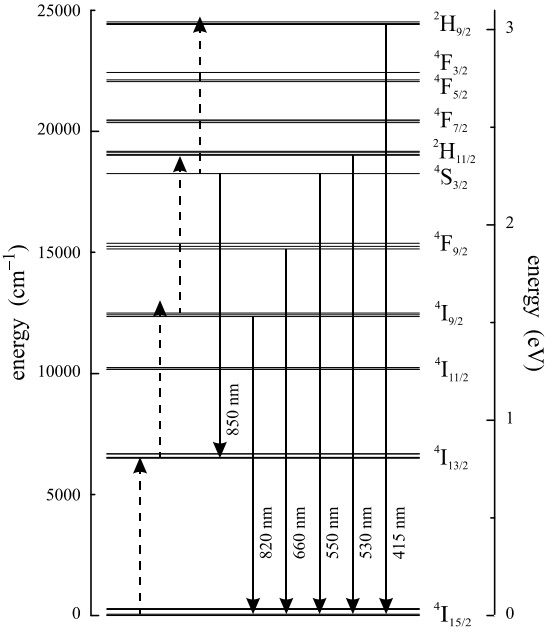

Figure 12 Energy level diagram of Er^{3+} in FZ glasses. Possible upconversion routes (dashed arrows) and assignments of the main upconverted emission bands (solid arrows) are indicated [15, 16].

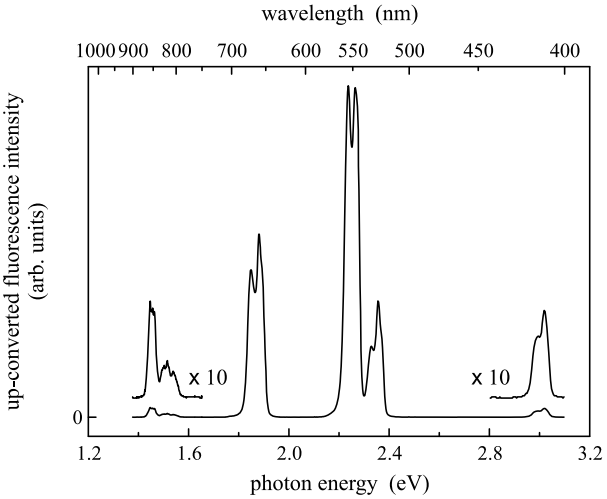

Figure 13 Upconverted fluorescence spectrum for the Er-doped FZ glass sample. The upconverted fluorescence was excited at 1540 nm with a continuous wave infrared laser diode.

The band at 850 nm is caused by a transition from the $^4S_{3/2}$ to the $^4I_{13/2}$ state [17]. Four-photon upconverted fluorescence can be observed at 415 nm; this emission which is barely observable arises from the $^2H_{9/2}$ state.

3 Upconversion system with Er-based material

The development of Er-doped fluorochlorozirconate (FCZ) glasses is in its infancy. However, it makes sense to develop concepts for system realisation, to set up the necessary characterization equipment and to test new systems in parallel. In this way, the new material can be tested immediately and optimized in an upconverter/solar cell system. For this reason, we developed a bifacial, crystalline silicon solar cell to serve as a test device for the upconverter material. As shown previously, upconversion is a non-linear process and the efficiency of the upconversion increases with increasing illumination. Therefore an upconverter system should operate under concentrated sunlight and the solar cell should be designed for high illumination densities. Small distances between the grid fingers, low background doping of the substrate and thin (100 µm) cells allow for

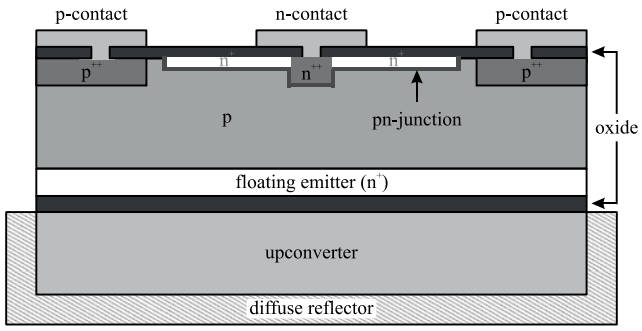

Figure 14 Bifacial solar cell with upconverter and diffuse back reflector for testing of the upconverter material. The system is illuminated from the top.

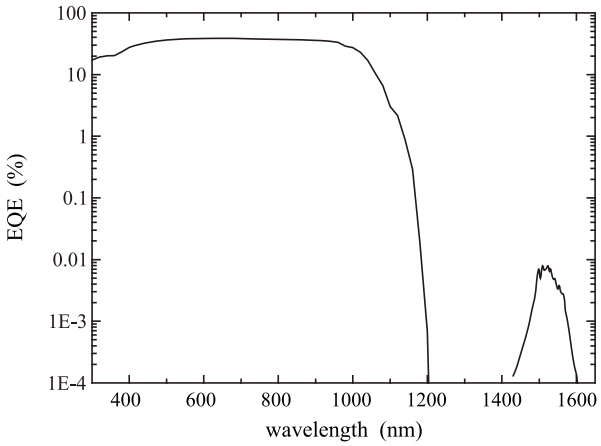

Figure 15 External quantum efficiency (EQE) of the upconversion system.

high efficiencies under concentrated conditions. To make application of different upconverter materials easy, enable a good optical coupling of upconverter and solar cell and to avoid any problems with the contacts, both contacts were placed on the front of the solar cell, which required an interdigitating pn-structure. The back is free of contacts (Fig. 14). The active cell area was 4.5×4.5 mm^2. This provides a very good test environment, but is not the highest efficiency design.

The spectral response of the new system was measured with a special setup: For this test we used $NaYF_4:20\%Er^{3+}$ powder as an upconverter, which was synthesized at the University of Bern by Krämer and Biner [18]. The powder was placed in a teflon mould, which serves as a back reflector and the solar cell was placed on top of the powder with the contact free side. We used a tuneable Santec ECL-210 laser to illuminate the system. The illumination intensity was 2.3×10^4 W/m^2 at 1523 nm. Since the upconversion efficiency depends non-linearly on the number of excitation photons, the photon flux was kept constant at approximately 1.6×10^{23} m^{-2} s^{-1} for all excitation wavelengths by controlling the laser power. The light was collimated and chopped and a lock-in amplifier was used to measure the short circuit current of the solar cell. A very low chopping frequency of 5 Hz was chosen because of the long radiative lifetime of the upconversion fluorescence. No white bias light was used. Figure 15 shows the quantum efficiency, calculated as the ratio of the short circuit currents of the upconversion system and a Ge reference cell in the spectral range from 1430 nm to 1630 nm. The quantum efficiency in the range from 300 nm to 1200 nm was measured using a xenon lamp with a double monochromator as an excitation source and a Si reference cell. The maximum quantum efficiency of the upconverter system was 8×10^{-3}%, between 1500 nm and 1530 nm.

4 Simulating the effect of selective amplification of transitions Both, our measured efficiency and also the efficiencies reported from [5] were achieved under illumination intensities, which correspond to concentration ratios of several thousand suns, especially when the photon fluxes in the absorption range of the upconverter are compared. In order to achieve these or higher efficiencies high concentration ratios have to be realized in a practical system. For this purpose external concentration by lenses or mirrors can be complemented by an internal, local intensity increase due to plasmon resonance in metal nanoparticles. In [19] it was shown that anisotropic Ag nanoparticles could enhance the photoluminescence emission of erbium by a factor of two. The nanoparticles were placed close to the Er ions and the dimension designed in a way that the plasmon modes are supported which are resonant with the erbium emission. Such an enhancement should be possible for the luminescence from upconversion processes when nanoparticles are incorporated into the glass ceramics.

The resonance frequency of the plasmons can be tuned by the size of the nanoparticles. In principal there are two options for the design frequency. On the one hand, one can aim for a direct enhancement of the emission of the upconverted photons by designing the nanoparticles so they support plasmons which are in resonance with the high energy transitions from the $^4I_{11/2}$ or $^4I_{9/2}$ erbium levels back to the ground level. On the other hand, one can aim for the enhancement of the absorption of the photons, by designing the nanoparticles so that the supported plasmons show resonance at the energy of the low energy photons, which should be absorbed. That is, the transitions $^4I_{15/2}$ to $^4I_{13/2}$ and $^4I_{13/2}$ to $^4I_{9/2}$ are amplified. To investigate which design has the largest impact on the upconversion efficiency, we developed a simulation model based on rate equations.

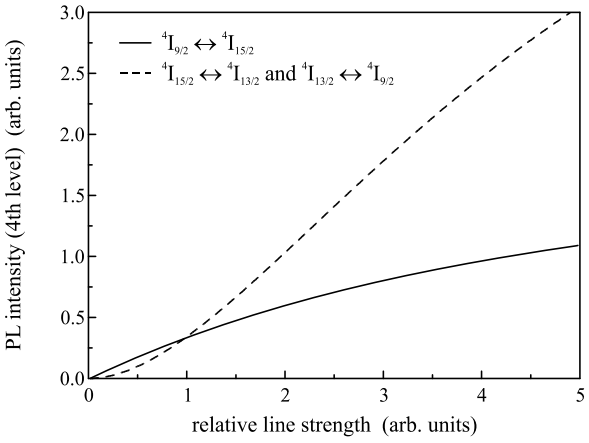

Figure 16 Emission relevant for the solar cell from the fourth level ($^4I_{9/2}$) to the ground state ($^4I_{15/2}$) vs. the relative line strength of the amplified transitions. Two cases are compared. In one case the line strength of the transition $^4I_{9/2} \leftrightarrow {}^4I_{15/2}$ has been amplified (solid curve), in the other case the "pumping" transitions $^4I_{15/2} \leftrightarrow {}^4I_{13/2}$ and $^4I_{13/2} \leftrightarrow {}^4I_{9/2}$ were amplified simultaneously (dashed curve). This graph shows the result for low excitation intensities of $0.0375 \cdot 4h\nu^3/c^3$. It becomes clear that for low energy densities it is more beneficial to amplify the "pumping" transitions.

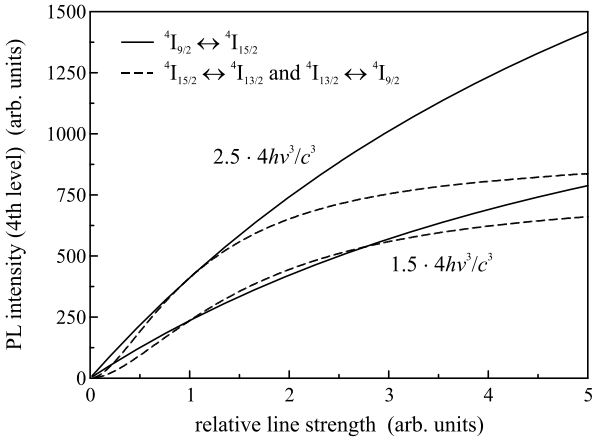

Figure 17 Same comparison as in Fig. 16, but this time for high excitation energy densities of $1.5 \cdot 4h\nu^3/c^3$ and $2.5 \cdot 4h\nu^3/c^3$. For this regime the amplification of the high energy transition is more beneficial.

The model describes the upconverter in equilibrium with a photon field with a spectral energy density, which has the dimension energy per volume per frequency unit. The model includes absorption, spontaneous emission and stimulated emission, which are described by the Einstein coefficients. Only upconversion via excited state absorption (ESA) is considered. A detailed description of the model will be given in [20]. We used this model to calculate the emission from the fourth level ($^4I_{9/2}$) to the ground state under excitation of the transitions from the $^4I_{15/2}$ to $^4I_{13/2}$ and $^4I_{13/2}$ to $^4I_{9/2}$. The relative line strengths of the various transitions were varied to simulate the effect of the plasmons. We compared two cases: In one case we increased the relative strength of the transition $^4I_{15/2} \leftrightarrow {}^4I_{9/2}$, in the other case the transitions $^4I_{15/2} \leftrightarrow {}^4I_{13/2}$ and $^4I_{13/2} \leftrightarrow {}^4I_{9/2}$ were increased simultaneously. Figures 16 and 17 display the results of the simulation for different illumination conditions.

Our simulations show that the amplification which results in the highest desired emission of upconverted light depends on the excitation energy density. The excitation spectral energy density may be expressed in terms of $4h\nu^3/c^3 = A/B$ (7.8×10^{-16} Js/m^3), A and B being the Einstein coefficients for spontaneous and stimulated emission, respectively; ν is the frequency of radiation used for the excitation. At energy densities below the threshold $4h\nu^3/c^3$ it is more beneficial to amplify the transitions of the desired absorption events. For excitation energy densities above the threshold more light is emitted when the transition of the desired emission is amplified directly. However, it has to be said that the threshold energy density of $4h\nu^3/c^3$ is a factor of 10^5 higher than the spectral energy of the sun at 1523 nm. A real system will work well below this level therefore we can state that the nanoparticles should be of a size that supports plasmon resonance at the frequencies of the upconverter absorption.

5 Conclusion Nd-doped FZ glasses which were additionally doped with chlorine ions show an increase in upconversion efficiency upon appropriate thermal processing. During the thermal processing hexagonal phase barium chloride nanocrystals are formed in the glass; the barium chloride volume fraction of the FCZ glass ceramic increases before it starts to decrease again for annealing temperatures above 270 °C. Upon annealing some of the Nd^{3+} ions enter the nanocrystals leading to splitting of the infrared fluorescence spectra and to increased upconverted fluorescence intensities. Again, the optimum value was found for the sample annealed at 270 °C for 20 min which agrees very well with the observation that this sample shows also the longest intermediate energy level lifetime.

We showed that Er is a promising candidate as an upconverter for silicon solar cells. However, upconversion efficiency needs to be increased. We will seek to achieve this increase by implementation of Er in FZ-glasses and by plasmon resonance. Our simulations show that the resonance frequency of the plasmons can be tuned so that they are in resonance with the desired absorption transitions of the upconversion.

Acknowledgements This work was supported by the FhG Internal Programs under Grant No. Attract 692 034. In addition, the authors would like to thank the Federal Ministry for Education and Research ("Bundesministerium für Bildung und Forschung") for their financial support (Verbundvorhaben: NanoVolt – Optische Nanostrukturen für die Photovoltaik). J. C. Goldschmidt gratefully acknowledges the scholarship support from the Deutsche Bundesstiftung Umwelt, and the ideational support from the Heinrich-Böll Stiftung and the German National Academic Foundation. The $NaYF_4:Er^{3+}$ upconverter was synthesized at the University of Bern by W. Krämer and D. Biner.

References

[1] B. Bendow, P. K. Banerjee, M. G. Drexhage, J. Goltman, S. S. Mitra, and C. T. Moynihan, J. Am. Ceram. Soc. **65**, C-8 (1982).
[2] P. N. Prasad, Nanophotonics (John Wiley & Sons, Hoboken, NJ, 2004).
[3] T. Trupke, M. A. Green, and P. Würfel, J. Appl. Phys. **92**, 4117 (2002).
[4] P. Gibart, F. Auzel, J. C. Guillaume, and K. Zahraman, Jpn. J. Appl. Phys. **35**, 4401 (1996).
[5] A. Shalav, B. S. Richards, T. Trupke, R. P. Corkish, K. W. Krämer, H. U. Güdel, and M. A. Green, Proceedings of the 3rd World Conference on Photovoltaic Energy Conversion, Osaka, Japan, 2003, p. 248.
[6] I. D. Aggarwal and G. Lu, Fluoride Glass Fiber Optics (Academic Press, London, 1991).
[7] B. Ahrens, C. Eisenschmidt, J. A. Johnson, P. T. Miclea, and S. Schweizer, Appl. Phys. Lett. **92**, 061905 (2008).
[8] A. Edgar, S. Schweizer, S. Assmann, J.-M. Spaeth, P. J. Newmann, and D. R. MacFarlane, J. Non-Cryst. Solids **284**, 237 (2001).

[9] G. Liu and H. A. Eick, J. Less-Common Met. **149**, 47 (1989).
[10] S. Schweizer, L. W. Hobbs, M. Secu, J.-M. Spaeth, A. Edgar, and G. V. M. Williams, Appl. Phys. Lett. **83**(3), 449 (2003).
[11] S. Schweizer, L. W. Hobbs, M. Secu, J.-M. Spaeth, A. Edgar, G. V. M. Williams, and J. Hamlin, J. Appl. Phys. **97**, 083522 (2005).
[12] P. Scherrer, Nachr. Ges. Wiss. Göttingen **2**, 98 (1918).
[13] J. Lucas, M. Chanthanasinh, M. Poulain, P. Brun, and M. J. Weber, J. Non-Cryst. Solids **27**, 273 (1978).
[14] B. Ahrens, B. Henke, J. A. Johnson, P. Miclea, and S. Schweizer, Proc. SPIE **7002**, 700206 (2008).
[15] A. T. Stanley, E. A. Harris, T. M. Searle, and J. M. Parker, J. Non-Cryst. Solids **161**, 235 (1993).
[16] G. H. Dieke and H. M. Crosswhite, Appl. Opt. **2**, 675 (1963).
[17] L. Wetenkamp, G. F. West, and H. Többen, J. Non-Cryst. Solids **140**, 35 (1992).
[18] K. W. Krämer, D. Biner, G. Frei, H. U. Güdel, M. P. Hehlen, and S. R. Lüthi, Chem. Mater. **16**(7), 1244 (2004).
[19] H. Mertens and A. Polman, Appl. Phys. Lett. **89**, 211107 (2006).
[20] P. Löper, J. C. Goldschmidt, M. Peters, D. Biner, K. Krämer, and S. W. Glunz, to be submitted (2008).

